Marine Geology 264 (2009) 16–27

Contents lists available at ScienceDirect

Marine Geology

journal homepage: www.elsevier.com/locate/margeo

Size distribution of submarine landslides along the U.S. Atlantic margin

Jason D. Chaytor [a,*], Uri S. ten Brink [b], Andrew R. Solow [c], Brian D. Andrews [b]

[a] Department of Geology and Geophysics, Woods Hole Oceanographic Institution, MS#24, Woods Hole, MA 02543, USA
[b] U.S. Geological Survey, Woods Hole Science Center, Woods Hole, MA, USA
[c] Marine Policy Center, Woods Hole Oceanographic Institution, Woods Hole, MA, USA

ARTICLE INFO

Article history:
Received 25 February 2008
Received in revised form 18 August 2008
Accepted 28 August 2008

Keywords:
bathymetry
inverse power-law
log–normal distribution
submarine geomorphology
landslide volume

ABSTRACT

Assessment of the probability for destructive landslide-generated tsunamis depends on the knowledge of the number, size, and frequency of large submarine landslides. This paper investigates the size distribution of submarine landslides along the U.S. Atlantic continental slope and rise using the size of the landslide source regions (landslide failure scars). Landslide scars along the margin identified in a detailed bathymetric Digital Elevation Model (DEM) have areas that range between 0.89 km^2 and 2410 km^2 and volumes between 0.002 km^3 and 179 km^3. The area to volume relationship of these failure scars is almost linear (inverse power-law exponent close to 1), suggesting a fairly uniform failure thickness of a few 10s of meters in each event, with only rare, deep excavating landslides. The cumulative volume distribution of the failure scars is very well described by a log–normal distribution rather than by an inverse power-law, the most commonly used distribution for both subaerial and submarine landslides. A log–normal distribution centered on a volume of 0.86 km^3 may indicate that landslides preferentially mobilize a moderate amount of material (on the order of 1 km^3), rather than large landslides or very small ones. Alternatively, the log–normal distribution may reflect an inverse power law distribution modified by a size-dependent probability of observing landslide scars in the bathymetry data. If the latter is the case, an inverse power-law distribution with an exponent of 1.3 ± 0.3, modified by a size-dependent conditional probability of identifying more failure scars with increasing landslide size, fits the observed size distribution. This exponent value is similar to the predicted exponent of 1.2 ± 0.3 for subaerial landslides in unconsolidated material. Both the log–normal and modified inverse power-law distributions of the observed failure scar volumes suggest that large landslides, which have the greatest potential to generate damaging tsunamis, occur infrequently along the margin.

1. Introduction

Recent evidence has shown the role of landslide-generated tsunamis to be of increasing importance in evaluating the hazard posed to coastal areas (e.g., Synolakis et al., 2002; Fine et al., 2005; Maramai et al., 2005; Greene et al., 2006; López-Venegas et al., 2008). By understanding the amount of material released in individual landslides, the distribution of landslides within a given geographic region, the recurrence time of landslides of particular sizes, and the mechanisms responsible for the generation of the landslides, we may be better able to determine that potential hazard of these events. Additionally, the derivation of size-distribution relationships for submarine landslides in many different geological environments provides valuable insight into the fundamental processes of landslide dynamics and margin evolution. Ultimately, the continued development of distribution relationships in areas of dense data coverage may aid in the estimation of the expected number of landslides of a particular size in a region from low data quality or incomplete observations.

Over the past several years, it has been suggested that the cumulative number-area and cumulative number-volume relationships of subaerial landslides can be described by inverse power-law distributions based on the dimensions of the failure scar, slide deposits, or headwall length (e.g., Sugai et al., 1994; Dai and Lee, 2001; Dussauge et al., 2003; Guthrie and Evans, 2004; Malamud et al., 2004). In the marine environment, the limited application of these statistical techniques for landslide analysis has resulted in only a few examples of such distribution relationships being observed (e.g., Issler et al., 2005; ten Brink et al., 2006; Micallef et al., 2008). Although power-law scaling is widely invoked to describe the distribution of subaerial and submarine landslide inventories, in the majority of these cases however, an inverse power-law distribution only applies to a truncated portion of mapped inventories. Undersampling of a particular range of magnitudes of landslide size is commonly suggested to account for the portion of the data that is not described by the inverse-power law function (see Guthrie et al., 2008 for a detailed discussion of this topic). Several methods have been employed to extend the fit of a power-law distribution to fully

* Corresponding author. Tel.: +1 508 457 2351; fax: +1 508 457 2310.
E-mail address: jason.chaytor@whoi.edu (J.D. Chaytor).

0025-3227/$ – see front matter © 2008 Elsevier B.V. All rights reserved.
doi:10.1016/j.margeo.2008.08.007

describe entire landslide inventories including the use of modified-pareto (e.g., Stark and Hovius, 2001) and gamma (e.g., Guzzetti et al., 2005) distributions and the application of different statistical techniques such as non-cumulative analysis and data binning (e.g., Burroughs and Tebbens, 2001; Guzzetti et al., 2002; Malamud and Turcotte, 2006). To date only a few examples of non-power-law distributions have been reported for landslides (e.g., logarithmic, Issler et al., 2005; log–normal, Dunning et al., 2007).

In this paper we investigate the cumulative size distribution of submarine landslide source zone (landslide failure scar) volumes identified along the different geologic provinces of the U.S. Atlantic continental margin (Fig. 1). Because this distribution differs from the classic inverse power-law usually determined for both subaerial and submarine landslides, we investigate potential causes of the departure, including variation of geologic conditions along the margin and observational bias. To obtain a more direct measure of the amount of material initially mobilized at the time of single failure we calculate volume and area of the failure scar, rather than the entire landslide (source and deposition regions) or the failure deposit only, as done in other similar studies (e.g., Issler et al., 2005). We have chosen this approach because many of the mapped landslide deposits are composite features resulting from multiple failures (Twichell et al., 2009-this issue). The generic term "landslide" throughout this paper encompasses all forms of submarine mass movement as described by Locat and Lee (2002) (i.e., slides, topples, spreads, falls, and flows).

1.1. Regional setting

The U.S. Atlantic margin (shelf, slope and rise) is covered by large volumes of Quaternary sediments eroded from the North American continent by glacial and fluvial processes. These sediments were deposited on a mix of Middle Jurassic carbonate, Eocene chalk, and other Mesozoic to Cenozoic siliclastic sedimentary formations that lie on the remnants of Triassic-Jurassic age rift basement (see Twichell

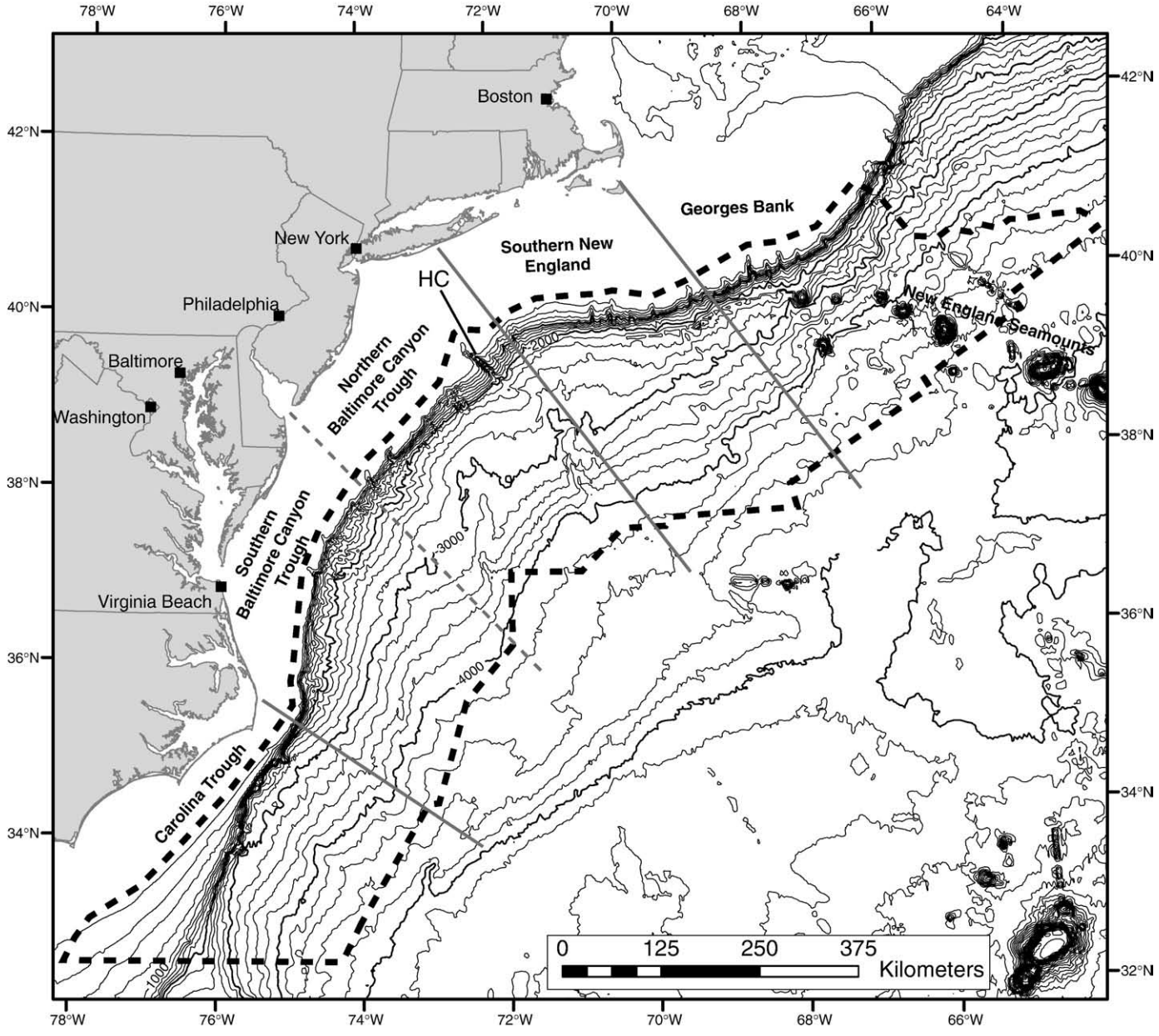

Fig. 1. Map of the U.S. Atlantic margin. The thick dashed line encloses the region in which source volume excavations were identified. The 5 geographic/geologic provinces as discussed in the text are also highlighted. HC — Hudson Canyon. Contour interval is 200 m.

et al., 2009-this issue for a more detailed overview of the margin's geology). Glacially-derived sediments deposited by large river systems are found along the Georges Bank shelf edge (Schlee and Fritsch, 1983) and along the shelf and slope/rise south of southern New England. South of the extent of glaciers, the large river systems that underlie the present Hudson, Delaware, and Chesapeake estuaries extended across the shelf with shelf-edge deltas built off the Virginia and Delaware coasts, while the Hudson Canyon system transferred sediment to a deep-sea fan (Poag and Sevon, 1989).

For the purpose of this study, we have separated the margin into five sub regions (Fig. 1), to explore the possibility of geologic control on the cumulative size distribution. Two of these regions are characterized by surficial glacial deposits on the shelf and slope (Georges Bank and Southern New England), one a mix of Quaternary fluvial deposits and exposed Eocene rock (Northern Baltimore Canyon Trough-NBCT), and the remaining two are characterized by surficial sediments of fluvial origin (Southern Baltimore Canyon Trough-SBCT) and from sediments carried by bottom currents that are deposited out of suspension (Carolina Trough).

2. Data and methods

We used a bathymetric Digital Elevation Model (DEM) with a grid-cell resolution of 100 m, derived from the compilation of multibeam swath bathymetry data from different sources and hydrographic soundings surveys (see Twichell et al., 2009-this issue for a full description of the bathymetry data), as the primary geographic dataset to identify the landslide source zones. The near-complete coverage of the U.S. Atlantic continental slope and rise by multibeam bathymetry provides a more uniform and detailed view of the geomorphology of submarine landslides than has been previously available. Although coverage is excellent, several significant gaps within the dataset totaling an area of approximately 26,000 km^2 (~8% of the total area) are present along the continental slope. Several major data gaps or areas of reduced resolution are present along the shelf edge and upper slope in the Georges Bank, Southern New England, and NBCT regions preventing the detailed or complete mapping of landslides that are only partially observed in these areas. In most cases, the identified failure scar appear to have been created by single evacuation events, but several of the scar, especially in the NBCT slope area, may have been created as either a single event or part of a larger retrogressive slide. In these cases, during the analysis, these slides were examined both as individual slides and as combined, larger single slides.

Landslide failure scar are identified through examining multiple perspective views of the bathymetric DEM using different illuminations, and the evaluation of seafloor slope maps derived from the DEM. The area of a failure scar is calculated as the planar area within a manually digitized bounding polygon that encompasses the region of negative elevation within the landslide's headwall and sidewalls. The downslope end of the failure scar is digitized as a straight line connecting the bounding sidewalls on either flank of the landslide, done in this way because the toe is usually obscured by slide deposits or cannot otherwise be identified on the bathymetry. Failure volumes were calculated using a method similar to ten Brink et al. (2006), in which a smooth upper surface is interpolated from the polygon that defines the boundary of each failure scar and is then subtracted from the extracted bathymetric data (lower surface) within a GIS (Fig. 2). The grid cell sizes of the upper and lower surfaces are each 100 m.

3. Landslide failure scar

A total of 141 landslide failure scars were identified within the ~347,000 km^2 investigated area of the U.S. Atlantic margin. Of these, 106 had sufficient data coverage and quality to assign high confidence values to their boundaries and as such they were used in the analysis (Figs. 3 and 4). The remaining failure scars that were not included in this analysis have only partial or lower-resolution coverage, with the area and volume values less reliable, but on average appear to be within the same size range as those used in the analysis. Measured areas for the scars range in size from 0.89 km^2 to a maximum of ~2410 km^2; with a total area for all scars of 15,275 km^2. Volumes range from as low as 0.002 km^3 up to ~179 km^3, with a margin-wide total removed volume of 862 km^3. It is currently not possible to determine if adjacent failure scars failed independently, together, or in a retrogressive manner. Booth et al. (1993) recognize that along the margin, landslides fall into two categories: 1) those with source areas on the continental slope and rise ("open-slope"); and 2) those that are sourced in submarine canyon and channel systems. In general, the largest values are from sources that displaced material on the open-slope rather than from the headwall and sidewalls of canyon and channel systems. While canyon/channel sources account for a significant portion of the total number of landslide failure scars that were identified and mapped (~30%) they constitute only ~6.5% and 7.1% of the total margin-wide mapped source zone area and volume, respectively.

Although the range of source zone area values is distributed across the margin, some local geographic clustering of values is noted (Fig. 5a), which may be a reflection of differing geological or geotechnical conditions along the margin, or a result of different regional triggering mechanism. The largest scar areas (>500 km^2) are found in three of the five geologic provinces, Georges Bank, SBCT, and

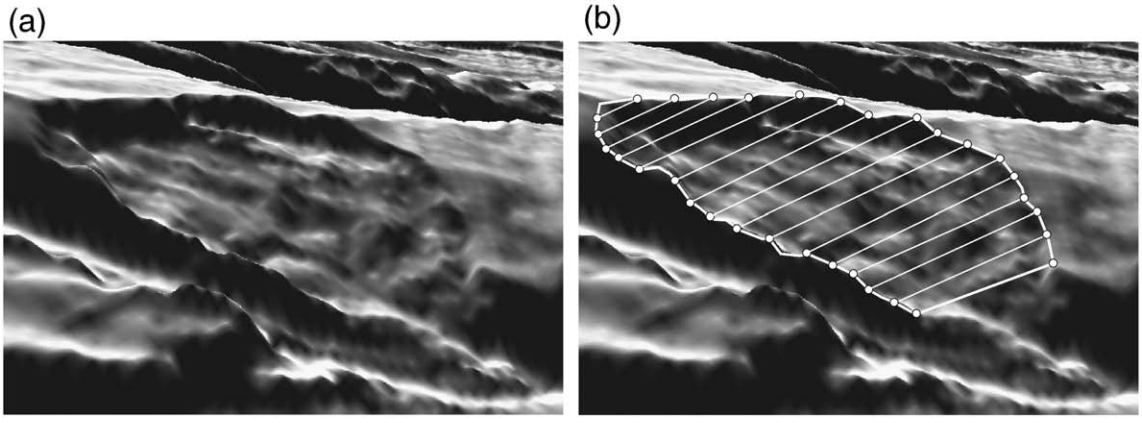

Fig. 2. Perspective view of a failure scar area (grey shaded bathymetry; ~10x vertical exaggeration) on the left, with a schematic example of the smooth-surface that was fit within the perimeter and used as the upper surface to estimate the excavated volume on the right.

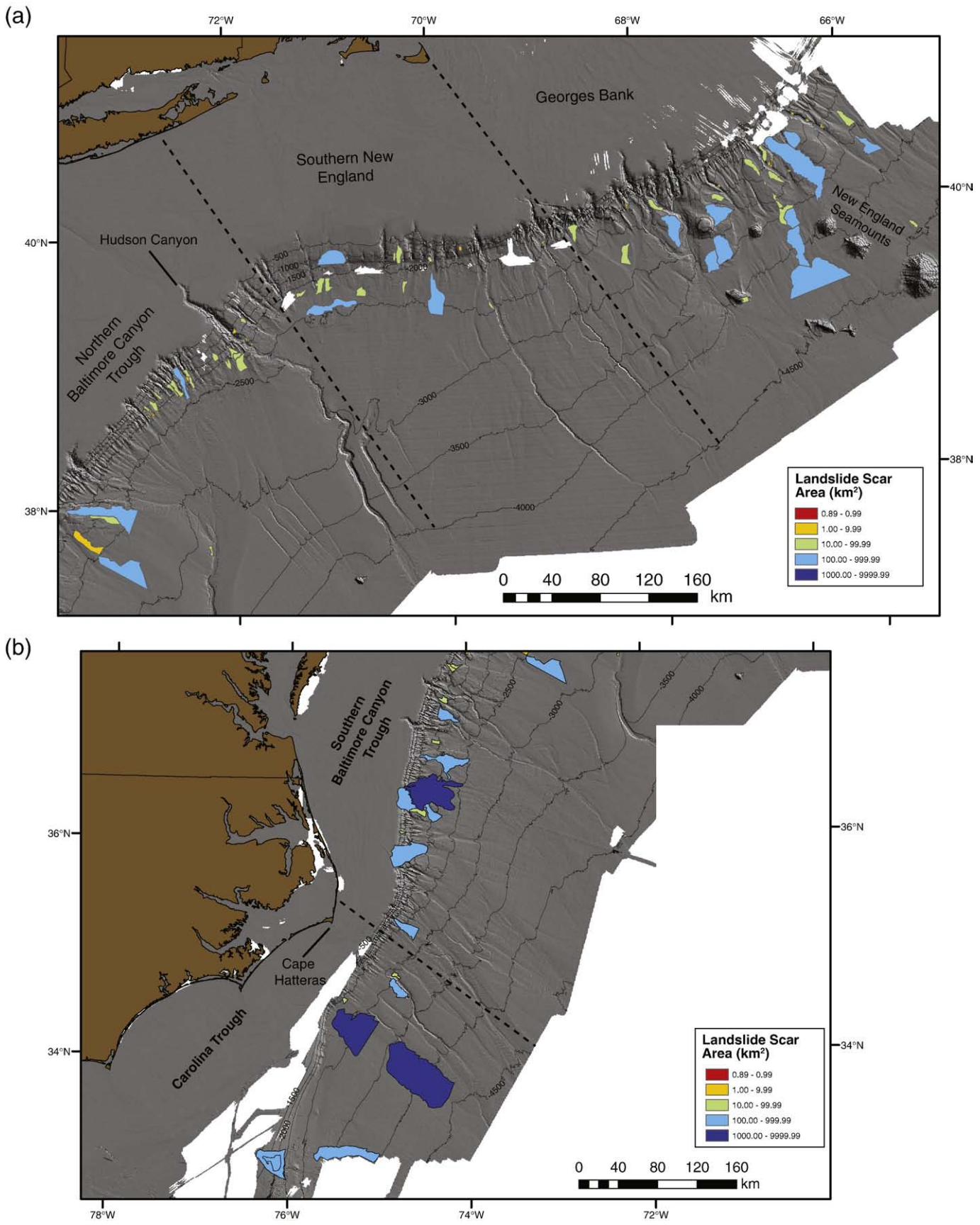

Fig. 3. Map showing the distribution of landslide failure scar area values across the (a) northern U.S. Atlantic margin and (b) southern U.S. Atlantic margin. Dashed black lines mark the boundaries of the geographic areas from Fig. 1. Contour interval is 500 m. DEM illumination is from the NE, with 2x vertical exaggeration.

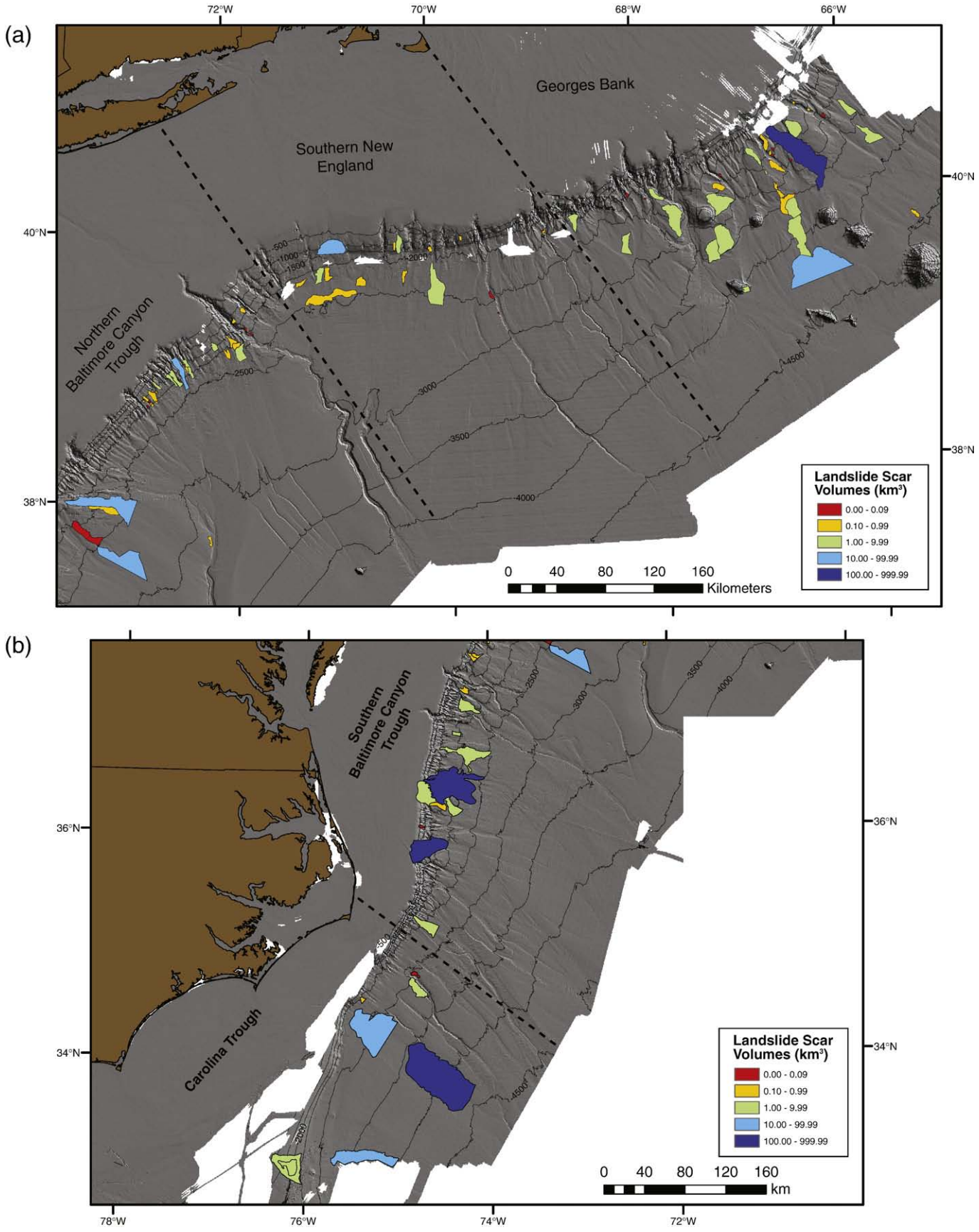

Fig. 4. Map showing the distribution of landslide failure scar volume values across the (a) northern U.S. Atlantic margin and (b) southern U.S. Atlantic margin. Dashed black lines mark the boundaries of the geographic areas from Fig. 1. Contour interval is 500 m. DEM illumination is from the NE, with 2x vertical exaggeration.

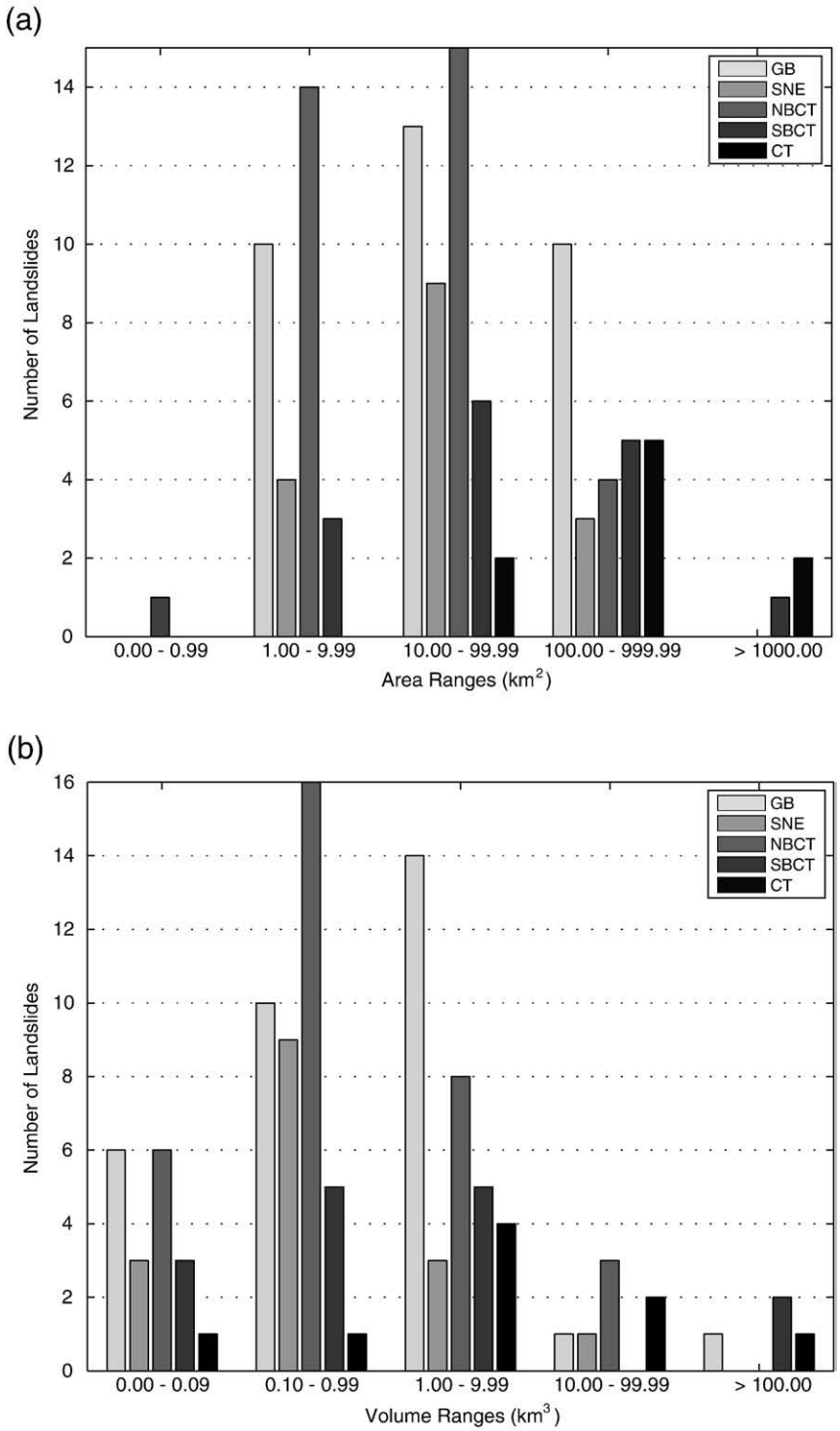

Fig. 5. Histograms of landslide source zone areas (a) and source zone volume (b) separated based on the five geographic regions shown in Fig. 1.

the Carolina Trough regions (Fig. 3a and b). All of these large scars are slope rather than canyon sources, although limited data availability in the Southern New England region prevents a full evaluation of that area. In the southernmost part of the SBCT and Carolina Trough regions (Fig. 3b), area values greater than 1000 km^2 are found, with few, if any, small-area sources. In contrast, failure scars with small areas (~<100 km^2) dominate the continental slope offshore of New York and New Jersey south of Hudson Canyon. Area values in the southern New England region are distributed well below 500 km^2, but the region may actually contain a greater number of landslide scars than currently observed, some with area values greater than 1000 km^2, especially along the sections of the slope where multibeam bathymetry data are missing or of limited resolution.

The full range of source zone volumes are also distributed across the margin (Fig. 4 and 5b), but with less obvious clustering than with the area values. Except for the two very large scars off Georges Bank, source volumes are characteristically in the 0.1 to 10 km^3 size range in the Georges Bank, southern New England, and NBCT regions,. The dominant range of source volumes in the southern NBCT, SBCT, and Carolina Trough regions covers the 0.1–100 km^3 range. As with the

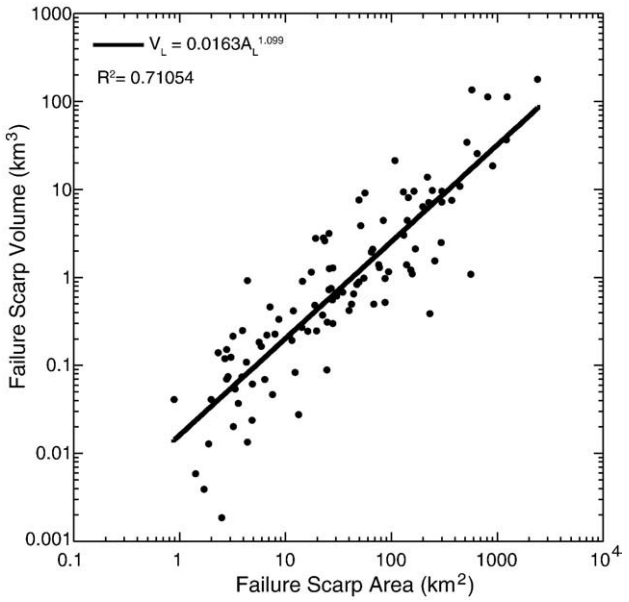

Fig. 6. Relationship between area and volume of the 106 failure scars along the U.S. Atlantic margin.

area values, the largest source volumes, those greater than 100 km^3, are found in the Georges Bank, SBCT, and Carolina Trough regions, but there is not a 1:1 relationship between regions with the largest areas and those with the largest volumes.

The area/volume relationship for U.S. Atlantic margin landslide source zones (Fig. 6; $V_L = 0.0163A_L^{1.099}$, $R^2 = 0.711$) is similar to that calculated for the submarine Storegga Slide [$V_L = 0.0267A_L^{1.032}$, calculated by ten Brink et al. (2006) from data in Haflidason et al. (2005)], which, like the Atlantic margin landslides, primarily involved the failure of a thin (10s of meters thickness) layer of clay-rich sediments. This differs from area/volume relationships previously calculated for both subaerial landslides (e.g., $V_L = 0.0240A_L^{1.368}$, Simonett, 1967) and submarine slope failures of carbonate rock around Puerto Rico (e.g., $V_L = 0.0263A_L^{1.292}$, ten Brink et al., 2006). The different exponent values can be explained by differences in the failed material and landslide processes or by the presence of saturated or overpressured sediments in the submarine environment. For small exponent values, such as that calculated for the Atlantic margin sources, volumes increase almost linearly with area, possibly resulting from a thin and relatively constant evacuation depth for each landslide, with the majority of landslides only mobilizing sediments within the unconsolidated Quaternary sedimentary section. This is in contrast to areas characterized by larger exponents, such as landslides on the margin of the Puerto Rico Trench and numerous subaerial slides, where thick sections of unconsolidated and consolidated material are evacuated during each event, resulting in the formation of rotational landslides, rock slides and falls, and debris avalanches. Such a marked difference in excavation depth in the source zone has

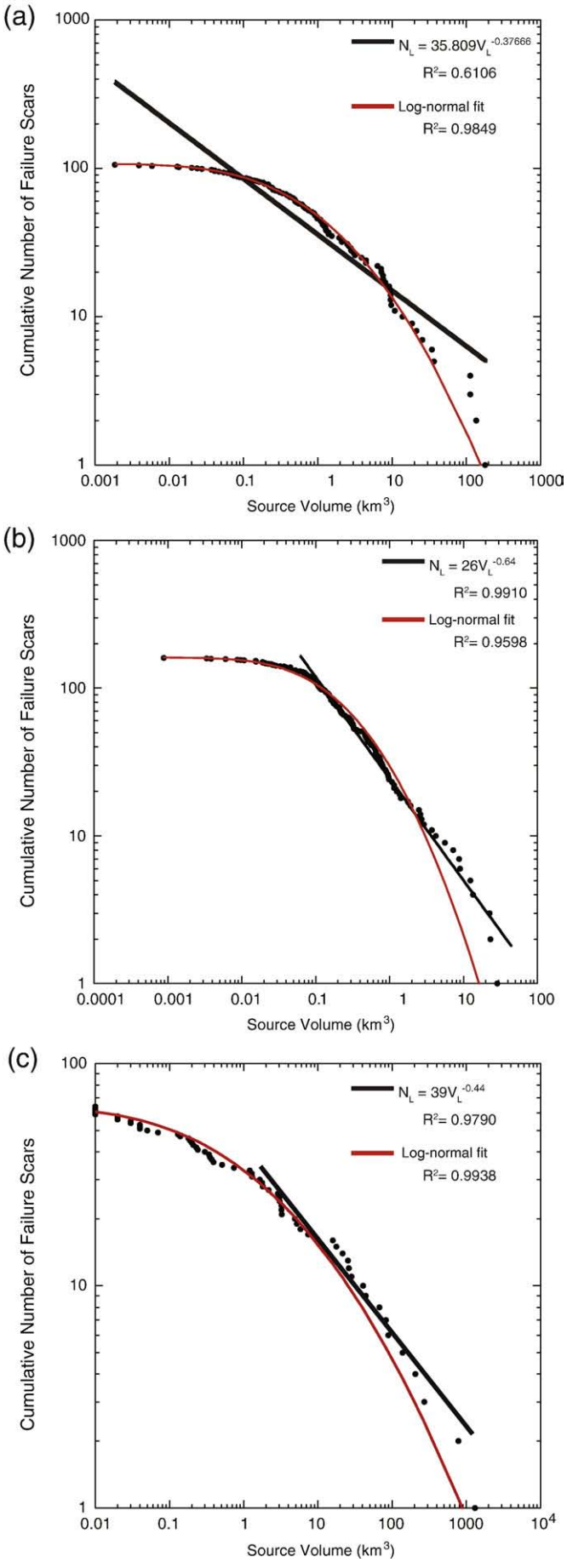

Fig. 7. (a) Log–log plot showing the cumulative volume distribution of 106 observed failure scars overlain by the poorly fitting calculated inverse power-law distribution (black line) and well-fit log–normal distribution (red line). (b) Log–log plot showing the cumulative volume distribution of landslide sources from Puerto Rico (data from ten Brink et al., 2006), showing the good fit of an inverse power-law distribution for volumes greater than ~0.1 km^3 (black lines) and the modeled log–normal distribution (red line). (c) Log–log plot showing the cumulative volume distribution of landslide sources from the Storegga Slide (data from Haflidason et al., 2005), showing the good fit of an inverse power-law distribution for volumes greater than ~2 km^3 (black lines) and the good fit of those data to a log–normal distribution (red line).

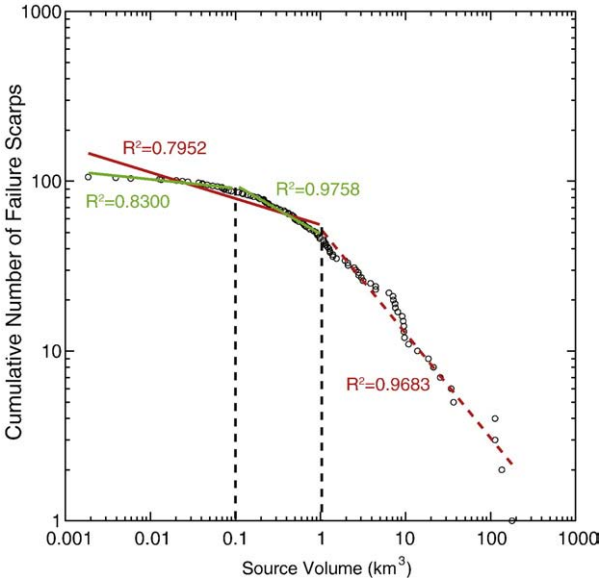

Fig. 8. Cumulative volume distribution of the 106 observed failure scars described by two (red solid and dashed lines) and three (green solid lines and red dashed line) showing that at best, a inverse power-law can only describe a truncated portion of the distribution over two or fewer orders of magnitude.

important implications for scar preservation and is discussed in the following section.

4. Size distribution of submarine landslides

4.1. Log–normal distribution

Because the volume of material that is released during a submarine landslide is one of the critical parameters controlling the amplitude of a landslide-generated tsunami (Pelinovsky and Poplavsky, 1997; Murty, 2003; Watts and Grilli, 2003; Geist et al., 2009-this issue), the following analysis is focused predominantly on the volumes of the failure scars. The observed volumes of the identified failure scars on the U.S. Atlantic margin plotted as a cumulative number on a log scale (Fig. 7) show a very good fit ($R^2 = 0.985$) to a log–normal distribution across the entire dataset, with a standard deviation (σ) and sample mean (μ) of log volume of 2.27 and 6.60, respectively. For the entire dataset, an inverse power-law provides a poor fit ($R^2 = 0.611$). That said, in some cases it has been possible to differentiate the mechanisms by which landslides are initiated and to describe complete landslide inventories by several power-law distributions (Van Den Eeckhaut et al., 2007). Attempts to describe the Atlantic margin landslide data in this way (Fig. 8) using arbitrary break-points loosely based on changes in the shape of the cumulative data curve, show that a robust inverse power-law distribution ($R^2 \geq 0.9$), can at best, only be applied over two orders of magnitude, providing a weak description of the entire inventory.

The differences in distributions of landslides along the U.S. Atlantic margin when compared to other regions mentioned above (i.e., log–normal vs. inverse power law) may reflect observational limitations or error, it may be due to a more fundamental characteristic of the study area, such as geologic control on the landslides, or it may be related to a dynamic feature of the landslide processes that controls their size. For example, in many regions, the variation of geomorphic, lithologic, or structural characteristics can be a critical factor in controlling the differences in the rate and magnitude of landscape modification by slope failure (Burbank and Anderson, 2001). The region under study here encompasses a very large geographic area, with variations in geology (e.g., Quaternary glacial and non-glacial fluvial deposits), seafloor slope, and potential local triggering mechanisms such as: 1) salt diapirism south of Cape Hatteras (Dillon et al., 1982); 2) water discharge movement along the slope off New Jersey (Robb, 1984); 3) sediment thickness and composition changes (e.g., Pratson and Laine, 1989); and 4) hydrate destabilization (Carpenter, 1981) which may provide some control on the size of landslides and hence their distribution.

Analysis of the individual geologic and geographic regions shown in Fig. 1 for power-law behavior shows that over limited orders of magnitude or for truncated portions of data from these regions, inverse power-laws can be fit (Fig. 9). However, the power-law exponents do not vary with geology in any discernable pattern. For example, the inverse power-law exponents for the Georges Bank and southern New England regions, both characterized by surficial glacial deposits, differ significantly (Fig. 9 a,b) even though they are geologically similar regions. On the other hand, the exponents for the southern New England and NBCT regions are similar (Fig. 9b,c), yet they are characterized by surficial glacial deposits and a mix of fluvial deposits and exposed Eocene chalk, respectively. Note also the small number of samples in a number of the regions, which make the fits statistically less robust.

While the dynamic processes involved in the initiation and evolution of each landslide likely play a role in determining the size of a landslide, similar processes are likely to be operating in areas of common geology and physical setting (e.g., surface slope, geomorphic setting). That said, although there are marked differences in the landslide process between canyon- and open slope-sourced slides that may influence the distribution of the combined dataset as a result of differences in sediment availability, seafloor slope, and triggering mechanism, no strong power-law relationship was obtained when canyon or slope landslides were analyzed separately (Fig. 10a). Similarly, the cumulative volume distribution of landslides originating in both glacially and non-glacially derived Quaternary sediments follow a similar distribution to that of the complete inventory (Fig. 10b).

4.2. Test for a power law distribution

Another explanation for the observed log–normal distribution is that it has been modified by a conditional probability to observe only certain-sized failure scars. The ability to observe a landslide depends on several factors such as the quality and resolution of data used to observe it and the level of preservation (e.g., morphology, age, type of material evacuated) of the individual landslides. The horizontal resolution depends on data density and grid size, which in this analysis is 100 m by 100 m. Therefore, the minimum size of failure scar that can be identified from these data, given that it must be visible in three or more cells, is 0.09 km^2. Vertical resolutions of modern deep water multibeam systems are commonly on the order of 1–2% of water depth, which therefore affects both the ability to identify the failure scar and the calculation of volumes.

Equally important in determining the observational potential is the temporal distribution of the landslides and the level of preservation of the features within the failure source zone (Malamud et al., 2004). Given sufficient time, the morphology of the failure scars and the entire landslide as a whole will change shape or degrade to a level where they will become unrecognizable as the remnant of a landslide, introducing a size bias into the observed landslide dataset. Several processes acting individually or together are responsible for this size bias including pelagic/hemipelagic sedimentation, turbidite sedimentation and erosion, and the masking of older, smaller landslide features by newer, larger landslides (but not vice-versa). Although smaller landslides are most likely to be affected or even completely removed by these mechanisms, the morphology of large landslides may be altered enough with time to change their dimensions and prevent close estimation of their original area and

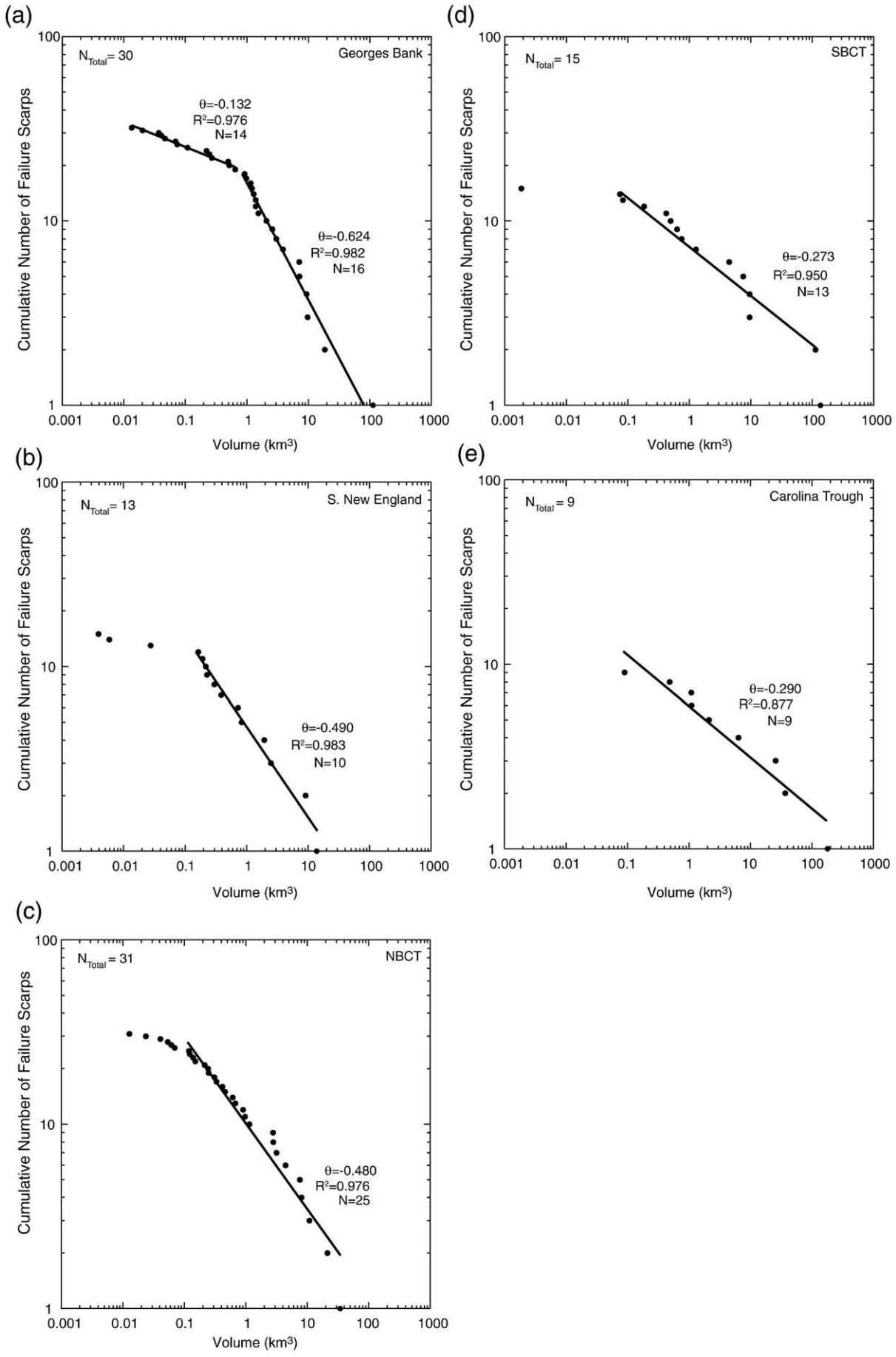
(a)
N_Total = 30
Georges Bank
θ=-0.132
R²=0.976
N=14
θ=-0.624
R²=0.982
N=16
Cumulative Number of Failure Scarps
Volume (km³)
(b)
N_Total = 13
S. New England
θ=-0.490
R²=0.983
N=10
(c)
N_Total = 31
NBCT
θ=-0.480
R²=0.976
N=25
(d)
N_Total = 15
SBCT
θ=-0.273
R²=0.950
N=13
(e)
N_Total = 9
Carolina Trough
θ=-0.290
R²=0.877
N=9

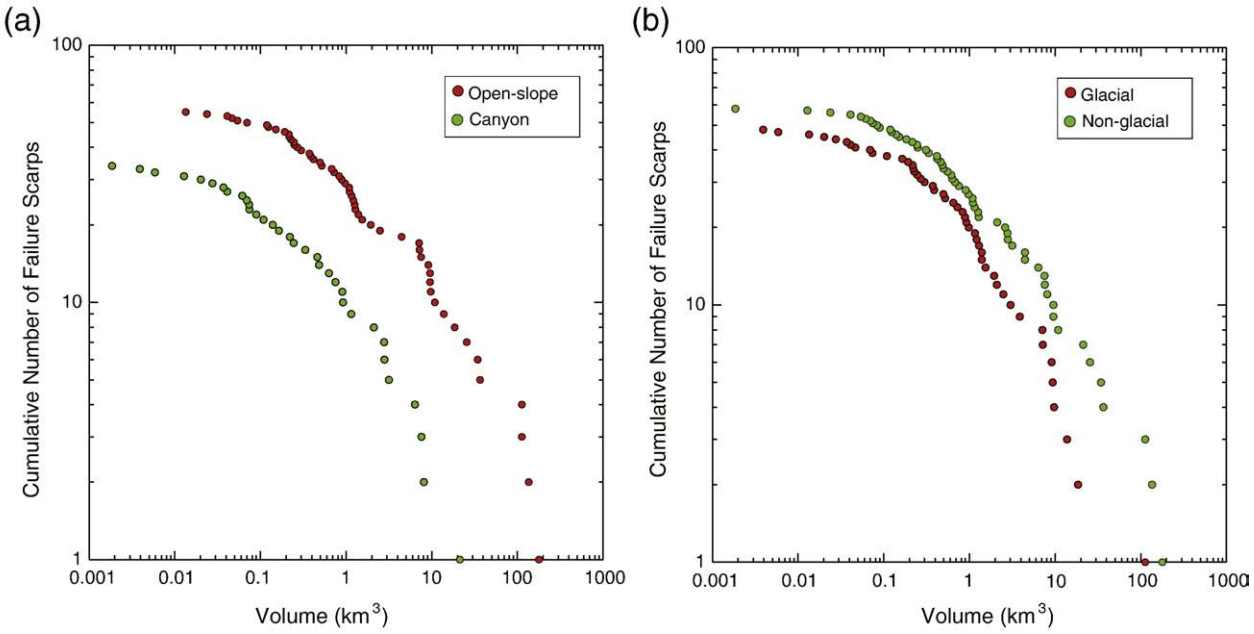

Fig. 10. Cumulative volume distributions of slope failures scars from (a) open-slope and submarine canyon environments and (b) glacial and non-glacial influenced depositional environments.

volume. On the U.S. Atlantic margin, all but one of the landslides that have reliable age information are pre-Holocene (Lee, 2009-this issue) so enough time may have passed for significant alteration of many of the failure scars. Additionally, the failure scar areas of the majority of the slides are wholly within the Quaternary sediments deposited on the continental slope, or within previously failed material on the continental rise, material that is more unstable and likely to degrade at a faster rate than slides sourced in a more coherent material such as a granite (Dussauge et al., 2003) or carbonate rock (ten Brink et al., 2006).

Let us assume that the cumulative-volume data should conform to a Pareto distribution for x, the volume of a landslide scar, with an inverse power-law exponent, θ:

$$F(x) = prob(X \leq x) = 1 - \left(\frac{x}{x_o}\right)^{-\theta} \quad (1)$$

where x_o is half of the minimum observed volume ($x_o = 0.001$ km^3 for U.S. Atlantic margin submarine landslides). Under this model:

$$\begin{aligned} \log\ prob(X \leq x) &= \log(1 - F(x)) \\ &= \psi - \theta \log x \end{aligned} \quad (2)$$

where $\psi = \theta \log x_o$.

To quantitatively investigate the possibility that those data presented here are size or observationally biased a conditional probability function is introduced. Observational bias means that the ability to identify landslide failure scars depends on the size of the scar. Using $Y = \log x$, the conditional probability density function of y, or the probability of identifying the failure scar, is:

$$g(y|\text{obs}) \propto p(\text{obs}|y) g(y) \quad (3)$$

where $p(\text{obs}|y)$ is the probability that a landslide scar of log volume y will be observed and $g(y)$ is the unconditional probability density of y, or the true size distribution of the landslide scars. If X has a Pareto distribution, then y has a truncated exponential distribution with a density function of:

$$g(y) = \theta e^{(-\theta(y - \ln x_o))} \quad y \geq \ln x_o \quad (4)$$

The shape of the conditional probability function $p(\text{obs}|y)$ for alternate values of the inverse power-law exponent θ, is derived from Eq. (3), giving:

$$p(obs|y) \propto \frac{g(y|obs)}{g(y)}. \quad (5)$$

For fixed values of x_o and θ, $p(\text{obs}|y)$ can be determined up to a scale constant by the ratio of an estimate of $g(\text{obs}|y)$ and $g(y)$. As previously mentioned, Fig. 7a shows the probability distribution of the observed log volume to be normal. Therefore under the normal approximation:

$$p(\text{obs}|y) \propto e^{\left(\theta y - \frac{1}{2}\left(\frac{y-\mu}{\sigma}\right)^2\right)}. \quad (6)$$

In other words, the observational probability will increase with increasing log landslide scar size y up to the point where $y = \mu + \sigma^2\theta$, then decline with increasing values of y (Fig. 11a). The standard deviation (σ) and sample mean (μ) of the log volume are 2.27 and 6.60, respectively.

Using Fig. 11a, some assumptions can be made to help determine an inverse power-law exponent (θ) for the distribution the submarine slides. Given that the median values of the landslide failure scar volume is 0.86 km^3, it is highly likely that a landslide failure scar volume of 1 km^3 or greater should be observed (i.e., a probability of observation > 0). Any exponent (θ) with a probability of observation of ~0 for failure scar volumes of 1 km^3 can therefore be rejected, which in this case occurs for $\theta \geq 1.6$ (Fig. 11a). Because the maximum possible size of landslides failure scars along the U.S. Atlantic margin is unknown, the maximum observed volume (179 km^3) is used to define the minimum θ. If it is assumed that the maximum failure scar should always be observed (probability of observation ~1), then only two values of θ have probabilities of observation high enough (>0.9) at this

Fig. 9. Cumulative volume distributions of slope failures scars from the five geographic/geologic regions as shown in Fig. 1 with the calculated goodness of fit and exponent of fitted inverse power-law: (a) Georges Bank, (b) Southern New England, (c) Northern Baltimore Canyon Trough (NBCT), (d) Southern Baltimore Canyon Trough, (e) Carolina Trough.

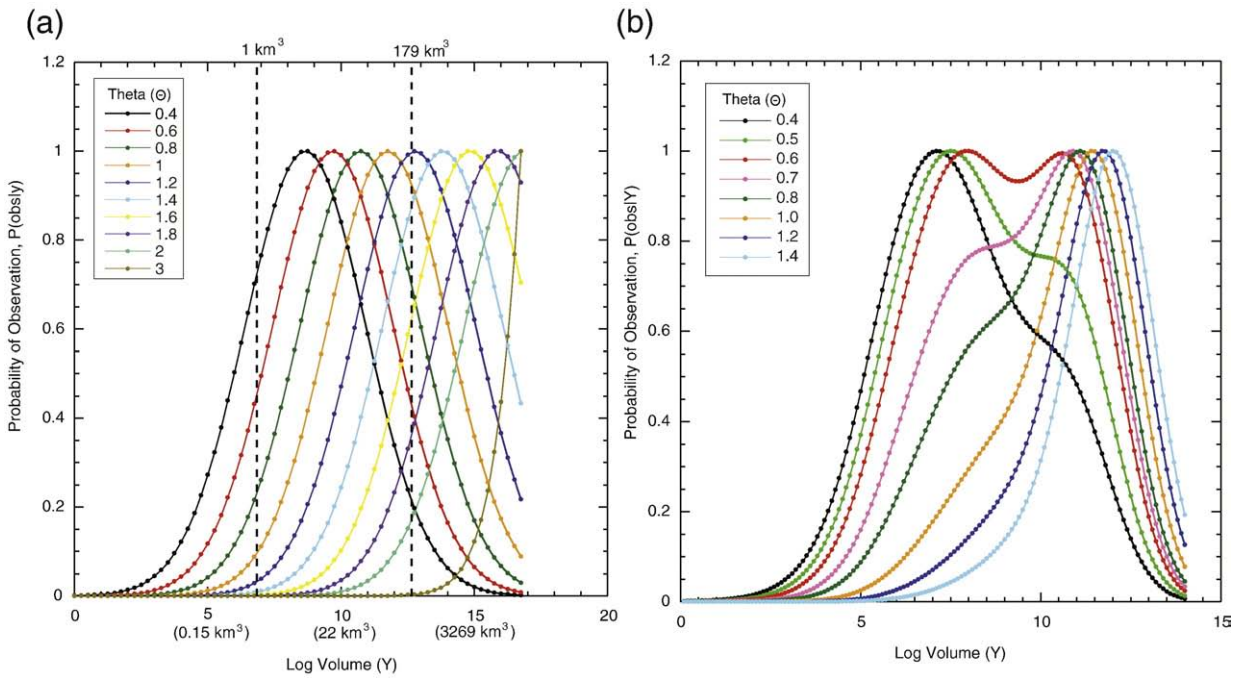

Fig. 11. (a) Probability of observation (normalized) versus log volume (Y) for U.S. Atlantic margin failure scar volumes for different power-law exponent values (θ). Values of θ that have an ~0 probability of observation above a volume of 1 km^3 are likely too high, while those that are not close to 1 for the maximum volume observed along the Atlantic margin are likely too small. Values in parentheses on the x-axis are the excavation volumes that correspond to the values of Y (i.e., $x = 0.001e^Y$). (b) Similar plot for the Puerto Rico data of ten Brink et al. (2006), where the flattening of the curves highlights the approximate best-fit value of θ (~0.6).

volume to satisfy the requirement, 1 and 1.2. Taking 1 as the minimum and 1.6 as the maximum, the estimated value of θ for landslide failure scars on the U.S. Atlantic margin is 1.3 ± 0.3. A similar plot analysis of observation probability for the Puerto Rico data (Fig. 11b) yields a value of θ of ~0.6, as is indicated by the near flattening of that curve at 1, very close to the 0.64 value calculated by ten Brink et al. (2006).

This range of exponent values is similar to the range of average cumulative distribution exponent values for the volumes of mixed-type subaerial landslides ($\theta = 1.2 \pm 0.3$) predicted by Dussauge et al. (2003). Furthermore, the calculated U.S. Atlantic margin distribution exponent is noticeably larger than that determined for submarine landslide sources in the carbonate platform surrounding Puerto Rico ($\theta = 0.64$; ten Brink et al., 2006), and for subaerial rockfall volumes ($\theta = 0.5 \pm 0.2$; Dussauge et al., 2003). The differences between the exponent values points toward the differences in cohesion and internal friction within the failed materials (Densmore et al., 1998; ten Brink et al., 2006). Provided that the distribution of landslides along the U.S. Atlantic margin can be described by a conditional probability of landslide observation, the inference of a large exponent value ($\theta > 1$) strengthens the interpretation that only the unconsolidated, mostly Quaternary, sediments and reworked landslide material (Twichell et al., 2009-this issue) are failing along the margin.

5. Possible causes for log–normal behavior

Fig. 7a shows that a log–normal distribution fits very well the cumulative volume distribution of submarine landslides along the U.S. Atlantic margin. Log–normal behavior has been observed in the frequency of natural events such erosion and depositional processes responsible for the creation of geomorphic features (Wolman and Miller, 1960), turbidite deposit bed volumes (Talling et al., 2007), in numerous biological mechanisms (Limpert et al., 2001), and earthquake recurrence (Nishenko and Buland, 1987). Except for a few cases (e.g., Dunning et al., 2007; Guthrie and Evans, 2007) log–normal behavior has not been invoked to describe landslide distributions even though both the landslides north of Puerto Rico (Fig. 7b) and especially those within the Storegga Slide complex (Fig. 7c) could be fit with log–normal distributions. Ultimately, one of the main reasons for examining the distribution of submarine landslides is to unravel the physical processes responsible for the distribution.

The nature of these controlling physical processes, both for subaerial and submarine landslides, are still under debate. For landslide distributions displaying power-law scaling, the concepts of self-organized criticality (SOC; Bak et al., 1988) or self-similarity have become popular (e.g., Noever, 1993; Guzzetti et al., 2002; Van Den Eeckhaut et al., 2007; Micallef et al., 2008). In this framework, landslides size distributions within the same system are thought to be scale invariant; essentially each landslide is a scaled copy of other landslides within a system that is in a critical state. But Gisiger (2001) and Solow (2005) show that power scaling cannot simply be taken as evidence for SOC, but rather criticality must be determined on a region-by-region basis. The fact that without modification, the entire identified landslide inventory along the U.S. Atlantic margin is not fit by an inverse power-law distribution, may imply that the failure process in the area does not obey SOC, but is indicative of a different processes. What these processes are remains to be determined, the answer may is likely to be the result of the interplay of a number variables, including the geology and geotechnical characteristics of a region, the nature of the triggering mechanism, and the dynamic behavior of the landslide once it has been initiated.

6. Conclusions

We showed that landslide source zone volumes along the U.S. Atlantic margin have a log–normal size distribution. This result, which fits very well across the entire data set, is in contrast to most analyses of landslide size distributions, which interpret an inverse power-law distribution over a truncated portion of data. Reanalysis of landslide debris-lobe volumes from the Storegga landslide complex were also found to show log–normal behavior across the entire inventory. A log–normal distribution suggests that landslides along the U.S. Atlantic margin have a characteristic volume of approximately 1 km^3. Both

large landslides and small landslides of less that 1 km^3 are less common along the margin, which may be a reflection of changes in geologic and geotechnical conditions along the margin or the type and magnitude of triggering mechanisms. To explore the possibility of size-dependant observational bias in identifying landslide failure scars in the bathymetry data, a conditional probability function was used together with an inverse power-law distribution to fit these data. The inverse power-law has an exponent value of 1.3 ± 0.3, which is close to that established for subaerial and submarine landslides in low cohesive, poorly consolidated material suggesting a similarity in excavation processes. In terms of the hazard posed by submarine landslides along the U.S. Atlantic margin, both the log–normal distribution of the observed source zone volumes suggest that large landslides, and the tsunamis that they can generate (e.g., 1929 Grand Banks landslide and tsunami; Piper et al., 1988), occur infrequently. Evaluation of this hypothesis awaits the collection of additional age data.

Acknowledgments

This work funded by U.S.-Nuclear Regulatory Commission grant N6480 Physical study of tsunami sources and the U.S. Geological Survey. Helpful comments which improved this manuscript were provided by David Twichell, Eric Geist, Thierry Mulder, David Piper, and an anonymous reviewer.

References

Bak, P., Tang, C., Wiesenfield, K., 1988. Self-organized criticality. Phys. Rev. A. 38, 364–374.
Booth, J.S., O'Leary, D.W., Popenoe, P., Danforth, W.W., 1993. U.S. Atlantic continental slope landslides: their distribution, general attributes, and implications. In: Schwab, W.C., Lee, H.J., Twichell, D.C. (Eds.), Submarine landslides: Selected studies in the U.S. Exclusive Economic Zone: U.S. Geological Survey Bulletin no. 2002, pp. 14–22.
Burbank, D.W., Anderson, R.S., 2001. Tectonic Geomorphology. Blackwell Science, Malden. 274pp.
Burroughs, S.M., Tebbens, S.F., 2001. Upper-truncated power laws in natural systems. Pure Appl. Geophys. 158, 741–757.
Carpenter, G., 1981. Coincident sediment slump/clathrate complexes on the U.S. Atlantic continental slope. Geo. Mar. Lett. 1, 29–32.
Dai, F.C., Lee, C.F., 2001. Frequency-volume relation and prediction of rainfall-induced landslides. Eng. Geol. 59, 253–266.
Densmore, A.L., Ellis, M.A., Anderson, R.S., 1998. Landsliding and the evolution of normal-fault-bounded mountains. J. Geophys. Res. 103 (B7), 15,203–15,219.
Dillon, W.P., Popenoe, P., Grow, J.A., Klitgord, K.D., Swift, B.A., Paull, C.K., Cashman, K.V., 1982. Growth faulting and salt diapirism: their relationship and control in the Carolina Trough, eastern North America. In: Watkins, J.S., Drake, C.L. (Eds.), Studies in continental margin geology. AAPG Memoir, vol. 34, pp. 21–46.
Dunning, S.A., Mitchell, W.A., Petley, D.N., Rosser, N.J., Cox, N.J., 2007. Landslides predating and triggered by the 2005 Kashmir earthquake: rockfall to rock avalanches. Geophys. Res. Abstr. 9, 06376.
Dussauge, C., Grasso, J., Helmstetter, A., 2003. Statistical analysis of rockfall volume distributions: implication for rockfall dynamics. J. Geophys. Res. 108 (B6), 2286. doi:10.1029/2001JB000650.
Fine, I.V., Rabinovich, A.B., Bornhold, B.D., Thomson, R.E., Kulikov, E.A., 2005. The Grand Banks *landslide*-generated *tsunami* of November 18, 1929: preliminary analysis and numerical modeling. Mar. Geol. 215, 45–57.
Geist, E.L., Lynett, P.J., Chaytor, J.D., 2009. Hydrodynamic modeling of tsunamis from the Currituck Landslide. Mar. Geo. 264, 41–52 (this issue).
Gisiger, T., 2001. Scale invariance in biology: coincidence or footprint of a universal mechanism? Biol. Rev. 76, 161–209.
Greene, H.G., Murai, L.Y., Watts, P., Maher, N.A., Fisher, M.A., Paull, C.E., Eichhubl, P., 2006. Submarine landslides in the Santa Barbara Channel as potential tsunami sources. Nat. Hazards Earth Syst. Sci. 6, 63–88.
Guthrie, R.H., Evans, S.G., 2004. Analysis of landslide frequencies and characteristics in a natural system, coastal British Columbia. Earth Surf. Process. Landf. 29, 1321–1339.
Guthrie, R.H., Evans, S.G., 2007. Work, persistence, and formative events: the geomorphic impact of landslides. Geomorphology 88, 266–275.
Guthrie, R.H., Deadman, P.J., Cabrera, A.R., Evans, S.G., 2008. Exploring the magnitude-frequency distribution: a cellular automata model for landslides. Landslides 5, 151–159.
Guzzetti, F., Malamud, B.D., Turcotte, D.L., Reichenbach, P., 2002. Power-law correlations of landslide areas in central Italy. Earth Planet. Sci. Lett. 195, 169–183.
Guzzetti, F., Reichenbach, P., Cardinali, M., Galli, M., Ardizzone, F., 2005. Probabilistic landslide hazard assessment at the basin scale. Geomorphology 72, 272–299.
Haflidason, H., Lien, R., Sejrup, H.P., Forsberg, C.F., Bryn, P., 2005. The dating and morphometry of the Storegga Slide. Mar. Pet. Geol. 22, 123–136.
Issler, D., De Blasio, F.V., Elverhoi, A., Bryn, P., Lien, R., 2005. Scaling behavior of clay-rich submarine debris flows. Mar. Pet. Geol. 22, 187–194.
Lee, H.J., 2009. Timing of occurrence of large submarine landslides on the Atlantic Ocean margin. Mar. Geol. 264, 53–64 (this issue).
Limpert, E., Stahel, W.A., Abbt, M., 2001. Log–normal distributions across the sciences: keys and clues. Bioscience 51 (5), 341–352.
Locat, J., Lee, H.J., 2002. Submarine landslides: advances and challenges. Can. Geotech. J. 39, 193–212.
López-Venegas, A.M., ten Brink, U.S., Geist, E.L., 2008. Submarine landslide as the source for the October 11, 1918 Mona Passage tsunami: observations and modeling. Mar. Geol. 254 (1–2), 35–46.
Malamud, B.D., Turcotte, D.L., 2006. An inverse cascade explanation for the power-law frequency-area statistics of earthquakes, landslides and wildfires. In: Cello, G., Malamud, B.D. (Eds.), Fractal Analysis for Natural Hazards. Geological Society, London, Special Publications 261, pp. 1–9.
Malamud, B.D., Turcotte, D.L., Guzzetti, F., Reichenbach, R., 2004. Landslide inventories and their statistical properties. Earth Surf. Process. Landf. 29, 687–711.
Maramai, A., Graziani, L., Alessio, G., Burrato, P., Colini, L., Cucci, L., Nappi, R., Nardi, A., Vilardo, G., 2005. Near-and far-field survey report of the 30 December 2002 Stromboli (Southern Italy) tsunami. Mar. Geol. 215, 93–106.
Micallef, A., Berndt, C., Masson, D.G., Stow, D.A.V., 2008. Scale invariant characteristics of the Storegga Slide and implications for large-scale submarine mass movements. Mar. Geol. 247, 46–60.
Murty, T.S., 2003. Tsunami wave height dependence on landslide volume. Pure Appl. Geophys. 160, 2147–2153.
Nishenko, S.P., Buland, R., 1987. A generic recurrence interval distribution for earthquake forecasting. Bull. Seismol. Soc. Am. 77, 1382–1399.
Noever, D.A., 1993. Himalayan sandpiles. Phys. Rev. E 47, 724–725.
Pelinovsky, E., Poplavsky, A., 1997. Simplified model of tsunami generation by submarine landslides. Phys. Chem. Earth 21, 13–17.
Piper, D.J.W., Shor, A.N., Hughes Clarke, J.E., 1988. The 1929 Grand Banks earthquake, slump and turbidity current. In: Clifton, H.E. (Ed.), Sedimentologic consequences of convulsive geologic events, Geological Society of America Special Paper 229, pp. 77–92.
Poag, C.W., Sevon, W.D., 1989. A record of Appalachian denudation in postrift Mesozoic and Cenozoic sedimentary deposits of the U.S. middle Atlantic continental margin. Geomorphology, 2, 119–157.
Pratson, L.F., Laine, E.P., 1989. The relative importance of gravity-induced versus current-controlled sedimentation during the Quaternary along the mideast U.S. Outer continental margin revealed by 3.5 kHz echo character. Mar. Geol. 89, 87–126.
Robb, J.M., 1984. Spring sapping on the lower continental slope, offshore New Jersey. Geology 12, 278–282.
Schlee, J.S., Fritsch, J., 1983. Seismic stratigraphy of the Georges Bank basin complex, offshore New England. In: Watkins, J.S., Drake, C.L. (Eds.), Studies in continental margin geology. AAPG Memoir, vol. 34, pp. 223–251.
Simonett, D.S., 1967. Landslide distribution and earthquakes in the Bewani and Torricelli Mountains, New Guinea; a statistical analysis. In: Jennings, J.N., Mabbutt, J.A. (Eds.), Landform Studies From Australia and New Guinea. Cambridge Univ. Press, Cambridge, pp. 68–84.
Solow, A.R., 2005. Power laws without complexity. Eco. Let. 8, 361–363.
Stark, C.P., Hovius, N., 2001. The characterization of landslide size distributions. Geophys. Res. Lett. 28, 1091–1094.
Sugai, T., Ohmori, H., Hirano, M., 1994. Rock control on magnitude-frequency distribution of landslides. Trans. Jpn. Geomorphol. Union 15, 233–251.
Synolakis, C.E., Bardet, J.-P., Borrero, J.C., Davies, H.L., Okal, E.A., Silver, E.A., Sweet, S., Tappin, D.R., 2002. The slump origin of the 1998 Papua New Guinea tsunami. Proc. R. Soc. Lond. A 458, 763–789.
Talling, P.J., Amy, L.A., Wynn, R.B., 2007. New insight into the evolution of large-volume turbidity current: comparison of turbidite shape and previous modeling results. Sedimentology 54, 737–769.
ten Brink, U.S., Giest, E.L., Andrews, B.D., 2006. Size distribution of submarine landslides and its implication to tsunami hazard in Puerto Rico. Geophys. Res. Lett. 33, L11307. doi:10.1029/2006GL026125.
Twichell, D.C., Chaytor, J.C., ten Brink, U.S., Buczkowski, B., 2009. Morphology of late Quaternary submarine landslides along the U.S. Atlantic continental margin. Mar. Geol. 264, 4–15 (this issue).
Van Den Eeckhaut, M., Poesen, J., Govers, G., Verstraeten, G., Demoulin, A., 2007. Characteristics of the size distribution of recent and historical landslides in a populated hilly region. Earth Planet. Sci. Lett. 256, 588–603.
Watts, P., Grilli, S.T., 2003. Tsunami Generation by Deformable Underwater Landslides. Proc. 13th Offshore and Polar Eng. Conf. (ISOPE03, Honolulu, USA, May 2003), pp. 364–371.
Wolman, M.G., Miller, J.P., 1960. Magnitude and frequency of forces in geomorphic processes. J. Geol. 68, 54–74.